Modeling of Springback Behavior in AA6016-T4 Sheet via an Elastoplastic Self-Consistent Model Incorporating Backstress.

Dane Sargeant¹, Md Zahidul², Rishabh Sharma³, Marko Kenezevic², David T. Fullwood³, Michael P. Miles¹

Abstract

Automotive stampings undergo complex strain paths during drawing, stretching and bending operations which develop large plastic strain gradients within the material. Aluminum sheet alloys are increasingly used for vehicle structure light-weighting, but limited formability and high levels of springback present challenges to the manufacturing and assembly processes. The current work explores the springback levels in AA6016-T4 sheet after pure bending operations. Finite element modeling is performed using both isotropic and elasto-plastic self-consistent (EPSC) crystal plasticity approaches. The EPSC model incorporates backstresses informed by GND content, as measured via high-resolution EBSD. Its predictions are shown to be more accurate than those of the isotropic model. The benefits and limitations of the current EPSC model are discussed.

Introduction

Forming operations are greatly influenced by the evolution of internal stresses during the deformation process. The redistribution of these stresses upon removal of plastic load causes springback in metals. Its physical effect manifests as elastic relaxation in the geometry of the final part. The necessity to completely understand the springback phenomenon is driven by the advances in forming techniques and the development of stronger materials that demonstrate greater springback. While the die adjustments to account for springback can be estimated via trial-anderror, it can be time-consuming and expensive requiring multiple tool geometries.

Finite element (models) can be employed to predict springback however, the accuracy of the model is dictated by the assumptions made by the inherent hardening law. The simple isotropic model assumes that the initial yield surface only has a radial expansion in the stress space which can be true for proportional loading conditions. On the contrary, under non-proportional loading, the kinematic model accounts for translation of the yield surface by including the backstress component. Previous studies have shown that while the isotropic model overestimates, the kinematic model with an average backstress tensor can underestimate springback. This discrepancy has been highlighted in the study by Eggertsen et al. which presents springback predictions from various models for four different steels under bending-unbending forming conditions using a three-point bending test [1]. They observed that the isotropic model over predicted the springback by 12% while Geng-Wagoner and Yoshida-Uemori kinematic hardening laws showed a deviation of 2% from the experimental results. In similar studies, Gau et al. [2] and Papeleux et al. [3] reported a maximum difference of 4° and 7°, respectively, in springback for 2D U-draw bending, predicted by their isotropic and kinematic model. Although these kinematic models' hardening laws incorporate necessary global backstress development to predict springback, they do not calculate local (grain-level) sources of backstress for an accurate forming response.

The current study employs a recently developed elasto-plastic self-consistent (EPSC) model, which incorporates local backstress development, to predict springback in AA6016-T4. The model has been previously employed and has been shown to accurately predict the cyclic loading and simple loading deformation in AA6022-T4. In the current paper, the EPSC predictions are assessed against experimental results and compared to an isotropic model to highlight the necessary effects of backstresses.

¹ Manufacturing Engineering Department, Brigham Young University, Utah, USA

² Mechanical Engineering Department, University of New Hampshire, New Hampshire, USA

³Department of Mechanical Engineering, Brigham Young University, Utah, USA

Experimental Results

The composition of the AA6016-T4 alloy provided by Commonwealth Aluminum, and used for the experimental work in this paper, is shown in Table 1. Stress-strain curves produced by uniaxial tension tests provided material properties and anisotropic behavior necessary for baseline comparisons and initial characterization. Specimens were cut from the sheet along the rolling direction (RD), transverse direction (TD), and 45° to the RD of the sheet according to the ASTM E8 specimen configuration in Figure 1. The specimens were pulled at a 1.5 mm/min crosshead displacement rate and the force-strain data were recorded using a load cell and extensometer. The specimens' thickness and width were recorded at five different points along the gauge length to accurately calculate applied stress.

Table 1 Nominal chemical composition of AA6016-T4

Sample	Al	Si	Mg	Fe	Mn	Zn	Cu	Ti	Cr
Al 6016	96.4-98.8	1.0-1.5	0.25-0.6	0-0.5	0-0.2	0-0.2	0-0.2	0-0.15	0-0.1



Fig. 1 ASTM E8 uniaxial tension specimen and dimensions in millimeters

Springback testing was completed by bending specimens on a 100-ton capacity Accurpress press-brake. Figure 2 shows tooling geometries for the punch and die set. Initial experiments employed bottom bending for unstrained and pre-strained samples. Bottom bending, which introduces full surface contact between the specimen and the V-die

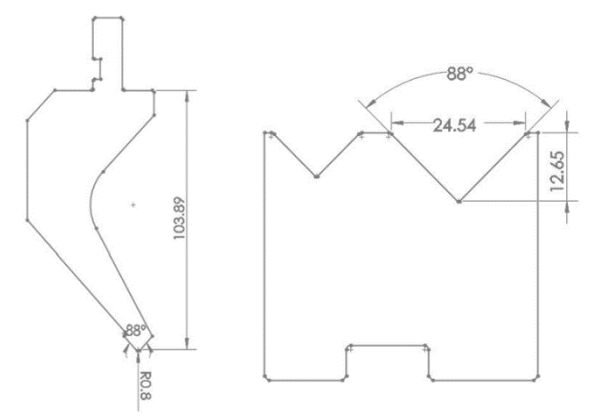


Fig. 2 Tooling geometries for pure bending operations. All dimensions are in millimeters

opening, requires a bending depth (BD) equal to the depth of the V-die (D) while considering the thickness of the material (T_m), as shown by eqn. 1. Depths beyond this value produce coining, which involves using enough tonnage to conform the sheet metal to the exact angle of the punch and die being used. In coining, the sheet metal is compressed and thinned at the bottom of the punch stroke, thus setting the shape of the part, and minimizing springback.

$$BD = D - T_m \tag{1}$$

To validate bottom bending results, each specimen was tracked via high-contrast HDR video recording through the duration of deformation at various bend depths (see Figure 3). Bend depths where the material and v-die did not maintain full contact, known as air bending, were disregarded. Thickness measurements were taken after presumed bottom bending experiments over five points along the specimen and compared to virgin material to ensure no thinning occurred.

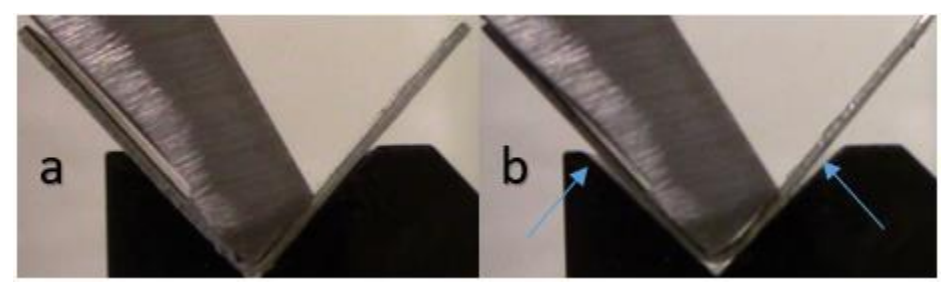


Fig. 3 HDR video recording snap-shots show bottom bending behavior (a) and air bending behavior (b) where material does not make full contact with v-die (blue arrows)

Springback was quantified through use of a VHX Keyence Digital Microscope. Upon unloading of the specimen, each was placed in a v-block centered on and parallel with the microscope stage edges. Through serial imaging performed at 20x zoom, the microscope measures the specimen from the bottom of the bend to the top specimen and produces a 2D profile map. (see Figure 4). Angles relative to the image profile were taken across three different sections for each sample and averaged together. This angle was compared to the angle of the V-die block and the springback levels were determined by taking the difference between the two angles, (i.e. measured angle minus die bend angle).

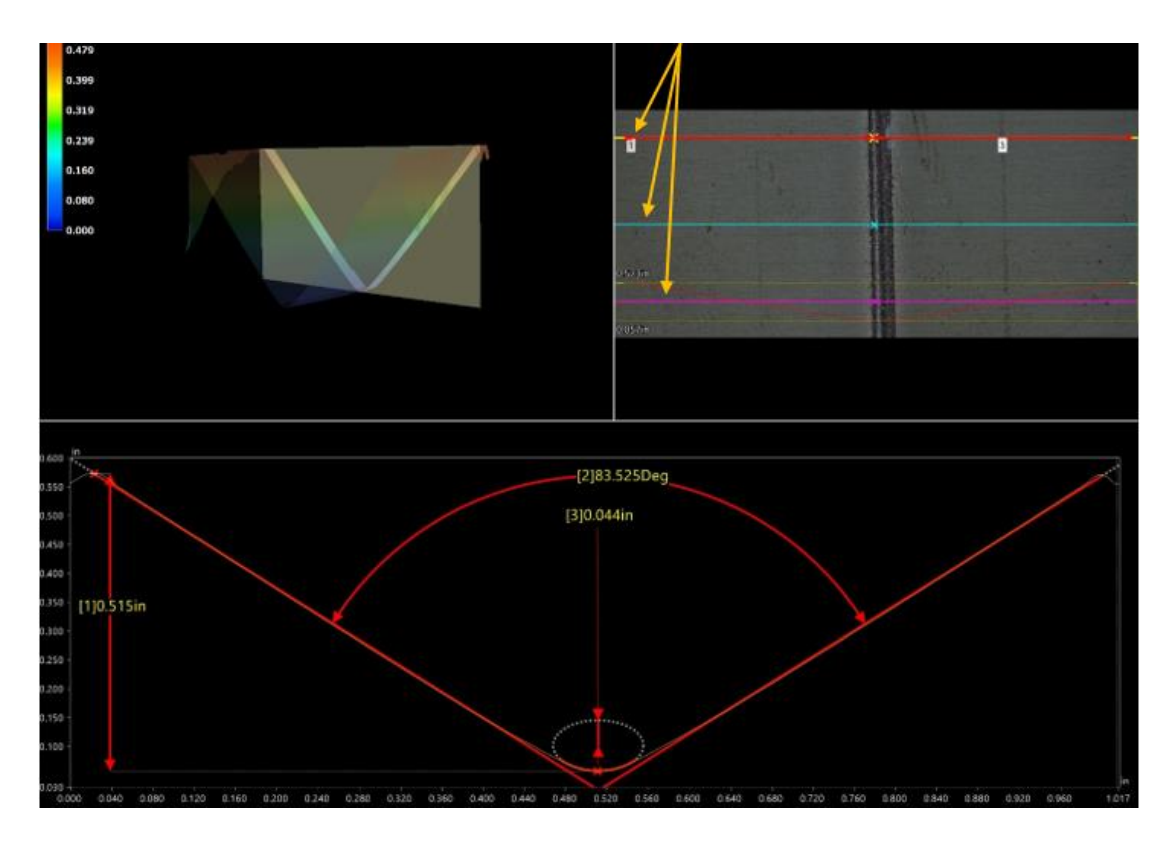


Fig. 4 VHX digital 2D profile map via serial sectioning at 20x zoom of AA6016-T4 sheet after bending. The three sections in the top right (*yellow lines*) indicate individual 2D profiles which were averaged together to get the relative angle after unload. This angle was used in springback calculations

Isotropic Finite Element Modeling

The springback experiments were replicated via finite element modeling with the ForgeNxT software, using an updated Lagrangian scheme with explicit time integration to model the forming of the sheet material, subjected to boundary conditions provided by the punch and the die. A plane-strain approximation was used to model the bending of the sheets, followed by a calculation of the final part shape after springback. An isotropic, elastio-viscoplastic material law was used to model the evolution of hardening in the material.

The sheet was discretized using an enhanced (P1+/P1) 3-noded triangular element, where equilibrium equations were solved at each increment using the Newton-Raphson method. The unilateral contact condition was applied to the sheet surfaces by means of a nodal penalty formulation, where the bending punch and the die were considered rigid.

Friction at the sliding interface between the sheet and the tool were modeled using a Coulomb law. The Coulomb friction law models shear stress at the contact interface as a function of contact pressure, or normal stress.

EPSC Model

A novel elasto-plastic self-consistent (EPSC) model, which incorporates grain-level backstress development, was used to predict the bending behavior of the sheet. The model treats a polycrystal as a collection of ellipsoidal grains with a specific crystallographic orientation and volume fraction. Overall properties of the polycrystal are obtained using the SC homogenization scheme in which each grain is considered as an elasto-plastic inclusion in the homogeneous-equivalent-medium (HEM). The properties of the HEM are those sought properties of the polycrystal. The particular modeling environment used in present work has been used for Al alloys in the past [4-6] as well as steels [6-8]. A detailed description of the aforementioned model as it applies to this paper can be found in [9]

Results & Discussion

The initial material characterization was performed under uniaxial tension. Minor differences were observed in the deformation response for RD, TD, and 45° to RD (Table 2). The strain-to-failure measured for the three orientations ranges from 0.24 to 0.27, with RD being the greatest.

Sample orientation	Young's modulus (GPa)	Strain-to-failure	Yield strength (MPa)	Ultimate tensile strength (MPa)
RD	70.5	0.27	142	344
45° to RD	70.8	0.245	140	321
TD	71.7	0.249	140	326

Table 2 Mechanical properties of AA6016-T4 under uniaxial tension true stress-strain curves

Springback experiments were performed with the bend axis perpendicular to the RD, TD and 45° to RD (Figure 5) orientations. Minor differences were observed in the springback response between the three bending orientations for both experimental and simulated response. The RD orientation exhibited a slightly higher springback value followed by TD and then 45° to RD, following the trend in UTS values in Table 2. The springback values produced were negative; this phenomenon known as "spring forward", arises during bottom bending as the material contacts the bottom of the die [10]. This type of elastic recovery is predominantly observed with the use of small punch tip radii and small bending angles, and causes the final angle of the sheet to be even smaller than that of the die [11].



Fig. 5 Bending samples oriented in the RD, TD, and 45° to RD direction. Samples are 2.5" [63.5mm] squares. Traverse line (black line) indicates the bend axis.

Isotropic modeling of the springback behavior exhibited opposite trends in relation to the orientations. Figures 6-8 depict a comparison between the isotropic simulation profile and the experimental specimen profiles for each orientation. Specimens oriented with the RD perpendicular to the bend axis exhibited slightly lower springback values, followed by TD and 45° to RD respectively. However, the predicted springback values differed by as much as 49% (1.8°) when compared to experimental data. The effect of a global backstress development incorporated into isotropic and kinematic hardening laws has been shown to produce such overestimations in springback [2-3]. Such an overestimate of final part geometry is detrimental for industrial applications where acute tolerances are required.

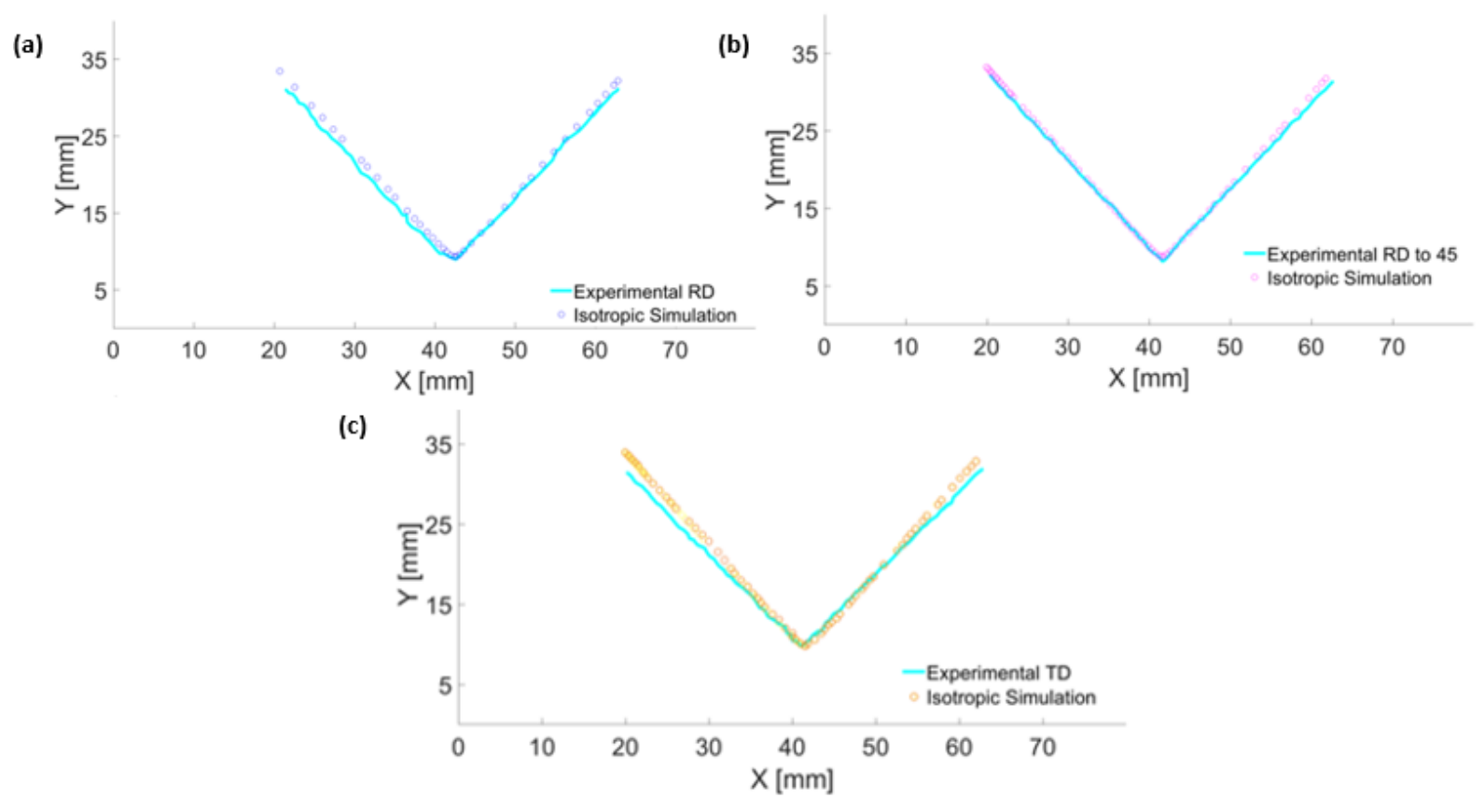


Fig. 5 Experimental vs isotropic simulation results in RD (a), TD (b), and 45° to RD (c)

The ESPC simulations were produced using ABAQUS finite element software utilizing three node configurations for appropriate modeling. An eight-node biquadratic (CPE8) plane strain element, an eight-node biquadratic with reduced (CPE8R) integration plane strain element, and a single four-node (CPE4) plane strain element type were compared. Boundary conditions and simulation setup for each node type were universal. Element conditions include zero

displacement in the z-direction for all nodes, including through-thickness nodes. The displacement in the z-direction of nodes not in the midplane is identical to the displacement of the corresponding nodes in the midplane. All simulations included 184 mesh elements (4-element through thickness) belonging to the plane strain family, and included a frictional coefficient of 0.05. Texture data was compacted to 100 grains for each orientation and used for simulation parameters. Texture inclusion as a parameter for the EPSC model is a key factor enabling. Figure 11 shows a comparison between all EPSC model profiles and the experimental data in the RD direction. CPE8R EPSC exhibited the closest fit to the experimental data. Figures 9-12 show the profile comparisons for the varying orientations and the CPE8R EPSC model fits against the experimental data.

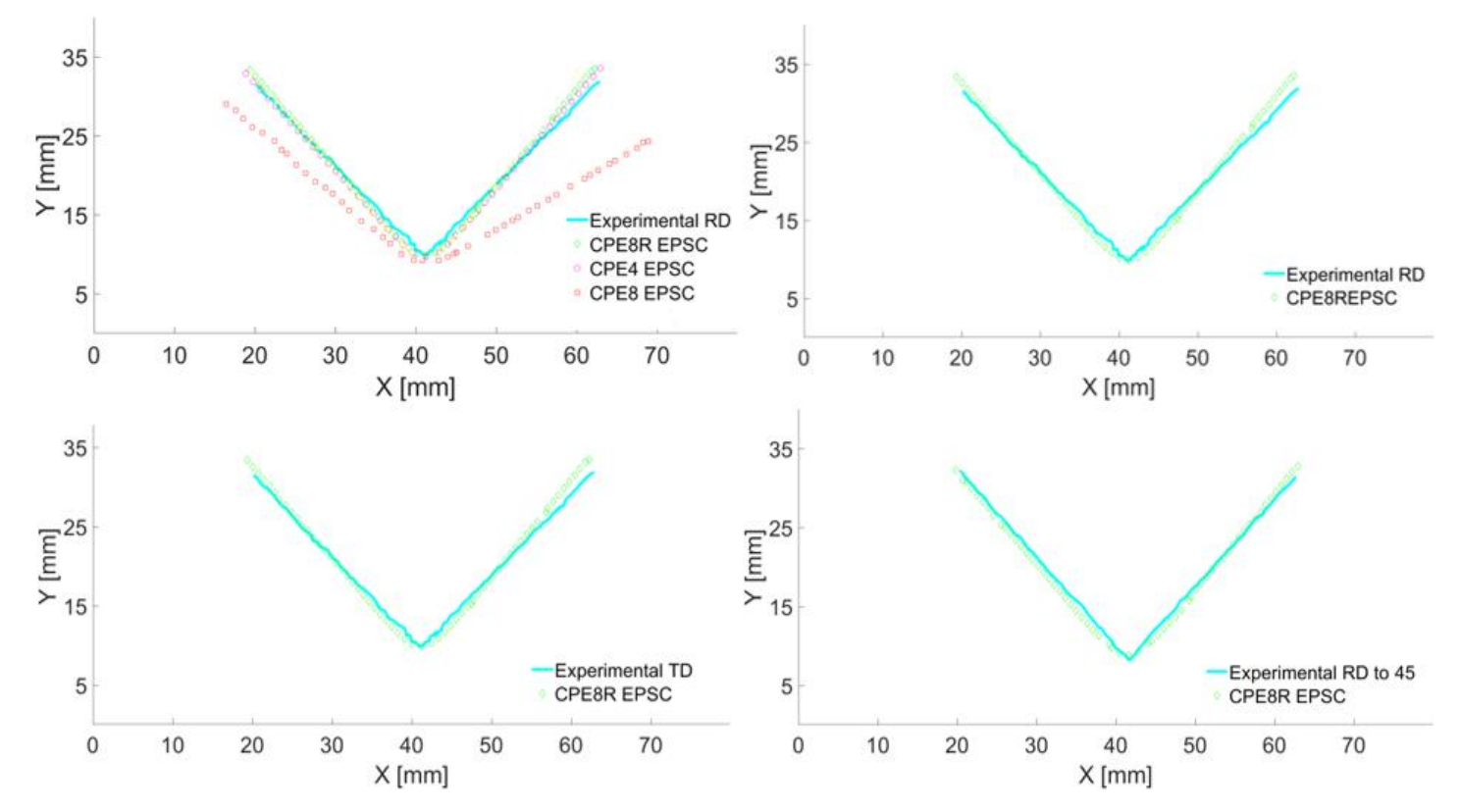


Fig. 6 Experimental vs all simulated EPSC results for texture orientation in RD (a), experimental vs CPE8R EPSC results for texture orientation in RD (b), TD (c), and 45° to RD (d)

Table 3 shows profile bent angles and springback values for experimental data, isotropic simulation data, and CPE8R EPSC simulation data respectively. The general trend follows the anisotropy of the material in that RD exhibits the largest amount of springback relative to the other orientations. The CPE8R ESPEC model captures the modeling behavior much more accurately with variations in springback compared to the experimental data no larger than 7% (0.3°).

Table 3 Springback value comparison between experimental data, EPSC model data, and Isotropic model data. for RD, TD, and 45° to RD.

Orientation	Experimental Bend Angle (°)	Springback Angle (°)	Isotropic Simulation Bend Angle (°)	Isotropic Simulation Springback Angle (°)		
RD	83.7	-4.3	82.9	-5.1	83.8	-4.2
TD	83.8	-4.2	82.4	-5.6	84.1	-3.9
45° to RD	83.9	-4.1	81.9	-6.1	84.1	-3.9

Conclusions

The current work employed both isotropic and elaso-plastic self-consistent modeling techniques against experimental

Key findings:

- Minor anisotropy in AA6016-T4 produces a slight variation in the springback behavior for RD, TD, and 45° to RD orientations.
- The EPSC model was able to match the experimental data well, with underestimation of springback by a maximum of 7%; and it also correctly accounted for the anisotropy for AA6016-T4.
- Isotropic modeling using an elastio-viscoplastic material law for evolution of hardening in the material showed overestimation of springback by as large as 49%, and was unable to account for anisotropy.
- Results show the inclusion of local backstress development at the texture/grain-level in the EPSC model enables the more accurate prediction and modeling of springback behaviors compared to a traditional isotropic hardening law [12].

References

- 1. Eggertsen, P.A. and K. Mattiasson, *On the modelling of the bending–unbending behaviour for accurate springback predictions.* International Journal of Mechanical Sciences, 2009. **51**(7): p. 547-563.
- 2. Gau, J.-T. and G.L. Kinzel, *A new model for springback prediction in which the Bauschinger effect is considered.* International Journal of Mechanical Sciences, 2001. **43**(8): p. 1813-1832.
- 3. Papeleux, L. and J.-P. Ponthot, *Finite element simulation of springback in sheet metal forming*. Journal of Materials Processing Technology, 2002. **125-126**: p. 785-791.
- 4. Zecevic, M. and M. Knezevic, A dislocation density based elasto-plastic self-consistent model for the prediction of cyclic deformation: Application to AA6022-T4. International Journal of Plasticity, 2015. 72: p. 200-217.
- 5. Zecevic, M. and M. Knezevic, *Latent hardening within the elasto-plastic self-consistent polycrystal homogenization to enable the prediction of anisotropy of AA6022-T4 sheets.* International Journal of Plasticity, 2018. **105**: p. 141-163.
- 6. Zecevic, M. and M. Knezevic, An implicit formulation of the elasto-plastic self-consistent polycrystal plasticity model and its implementation in implicit finite elements. Mechanics of Materials, 2019. **136**: p. 103065.
- 7. Zecevic, M., et al., *Dual-phase steel sheets under cyclic tension–compression to large strains: experiments and crystal plasticity modeling.* Journal of the Mechanics and Physics of Solids, 2016. **96**: p. 65-87.
- 8. Cantara, A.M., et al., *Predicting elastic anisotropy of dual-phase steels based on crystal mechanics and microstructure.* International Journal of Mechanical Sciences, 2019. **151**: p. 639-649.
- 9. Sharma, R.S., Dane; Darujo, Sowmya; Knevevic, Marko; Miles, Michael; Fullwood, David;, *Multi-strain path deformation behavior of AA6016-T4: Experiments and crystal plasticitymodeling*. International Journal of Solids and Structures, 2021.
- 10. Benson, S. *Bending Basics: The hows and whys of springback and springforward*. [Article] 2014 July 9, 2014 [cited 2021 7/8/2021]; Available from:

 https://www.thefabricator.com/thefabricator/article/bending/bending-basics-the-hows-and-whys-of-springback-and-springforward.
- 11. Bakhshivash, S., et al., Effect of Bending Angle and Punch Tip Radius on Spring-Forward in an Al-Mg-Si Alloy. 2016.
- 12. Zecevic, M., I.J. Beyerlein, and M. Knezevic, *Coupling elasto-plastic self-consistent crystal plasticity and implicit finite elements: applications to compression, cyclic tension-compression, and bending to large strains.* International Journal of Plasticity, 2017. **93**: p. 187-211.